Ideal strength and phonon instability in single-layer MoS_2

Tianshu Li*

Department of Civil and Environmental Engineering, George Washington University, Washington, DC 20052 USA

(Received 14 March 2012; revised manuscript received 13 May 2012; published 4 June 2012)

Ideal tensile stress strain relations for single-layer MoS_2 are investigated based on first-principle calculation, for biaxial tension and uniaxial tension along zigzag and armchair directions. The predicted ideal tensile strengths and elastic moduli are in excellent agreement with the very recent experimental measurements of Bertolazzi *et al*. [ACS Nano **5**, 9703 (2011)] and Castellanos-Gomez *et al*. [Adv. Mater. **24**, 772 (2012)]. It is identified that the tensile strength of single-layer MoS_2 are dictated by out-of-plane soft-mode phonon instability under biaxial tension and uniaxial tension along the armchair direction. This failure mechanism, different from that of the truly two-dimensional material graphene, is attributed to the out-of-plane atomic relaxation upon tensile strain. Investigation of the electronic structures of single-layer MoS_2 under tensile strain shows the material becomes an indirect semiconductor at small tensile strain (<2%) and turns into metallic before reaching the ideal tensile strength.

DOI: 10.1103/PhysRevB.85.235407 PACS number(s): 62.25.−g, 62.20.−x, 63.20.D−, 63.22.Np

Single-layer transition-metal dichalcogenides attracted intensive attentions in the recent years, due to the search for alternative two-dimensional (2D) material systems. Unlike graphene, which is intrinsically a gap-less semiconductor, single-layer MoS_2 has a direct energy gap of 1.8 eV.[1,2] Upon thinning from the bulk,[3–5] the electronic structure of MoS_2 undergoes an interesting transition. The variation of the electronic structure with the number of layers was investigated by first-principle calculation,[6] and the prediction was confirmed by photoluminescence experiments.[1,2] A recent experiment further demonstrated that single-layer MoS_2 has high intrinsic electron mobility and high on/off ratios.[7] These ideal properties make single-layer MoS_2 a very promising candidate for next generation field-effect transistors,[8] opto-electronics, and energy harvesting materials.

Just like graphene,[9,10] single-layer MoS_2 is also a promising material for flexible electronics. Previous theoretical studies[11,12] suggested single-layer MoS_2 nanoribbons have high structural stability and promising electronic and magnetic properties. Therefore, it is important to understand the elastic limit of single-layer MoS_2 and how its electronic structure varies with strain. While graphene is a truly 2D material, single-layer MoS_2 is composed of three atomic layers S-Mo-S (see Fig. 1). Therefore, the out-of-plane atomic relaxation upon in-plane tensile strain, which is absent in graphene, will likely play a role in the mechanical response of single-layer MoS_2. The mechanical properties of single-layer MoS_2 has been recently measured in nanomechanical experiments.[13,14] It was reported[13] that single-layer MoS_2 breaks at the maximum tensile stress of 22 ± 4 GPa, a stress level close to the estimated ideal strength based on the measured in-plane Young's modulus. The critical tensile strain was further estimated to be 0.06∼0.11 by assuming linear stress-strain relationship. Therefore, two questions arise from the experimental results: (1) Is the ideal strength attainable in single layer MoS_2? (2) If so, what is the limit of elastic strain, and how does it fail when approaching such limit? To answer both questions, here we employed first principle *ab initio* calculations to investigate the intrinsic mechanical responses to tensile strain in single-layer MoS_2. It is demonstrated here that the tensile strengths under biaxial and uniaxial along the armchair directions are in fact dictated by out-of-plane soft-mode phonon instability.

Our first principle calculations were carried out with Quantum-Espresso package[15] using Perdew-Burke-Ernzerhof functional[16] and Trouiller-Martins type norm-conserving pseudopotentials[17] with an energy cutoff of 100 Ry for the wave functions. A unit cell containing three atoms with one Mo atom and two S atoms (see Fig. 1) was chosen with the periodic boundary condition applied. To model single-layer MoS_2, a vacuum space of 10 Å was left along z direction, in order to avoid suspicious interactions between the periodic images. A Monkhorst-Pack grid of $20 \times 20 \times 1$ was used to sample the first Brillouin Zone. These parameters ensure the errors in the calculated total energy and stress components are less than 0.5 meV and 0.01 GPa, respectively.

The theoretical stress-strain relation were predicted by the first principle calculations by following a standard method.[18,19] We considered three loading conditions: uniaxial tension along x direction, i.e., the nearest Mo-Mo direction or the zigzag direction; uniaxial tension along y direction, i.e., the second-nearest Mo-Mo direction or the armchair direction; and biaxial tension. To compute the stress strain relationship, we apply a series of incremental tensile strain to the single-layer MoS_2 and relax the lattice along the orthogonal directions so that each of the corresponding conjugate stress components is less than 0.01 GPa. Because a vacuum space is left along the z direction in the unit cell, the calculated in-plane stress components must be rescaled[20] based on the effective layer thickness d_0 of single layer MoS_2. In order to make connections with experiments, we chose $d_0 = 6.145$ Å, i.e., one half of the out-of-plane lattice constant of MoS_2,[21] and rescale the in-plane stress components by h/d_0, where h is the length of the cell along z axis.

Figure 2 shows the calculated ideal tensile stress strain relations for the single-layer MoS_2 under both uniaxial and biaxial load conditions. By fitting the initial stress strain curves based on linear regression up to 2% strain (Fig. 2, inset), we obtained the corresponding elastic moduli $E_x = 197.9 \pm 4.3$ GPa and $E_y = 200.3 \pm 3.7$ GPa. The near degeneracy of the elastic moduli along two orthogonal directions implies that the single-layer MoS_2 is a virtually elastic

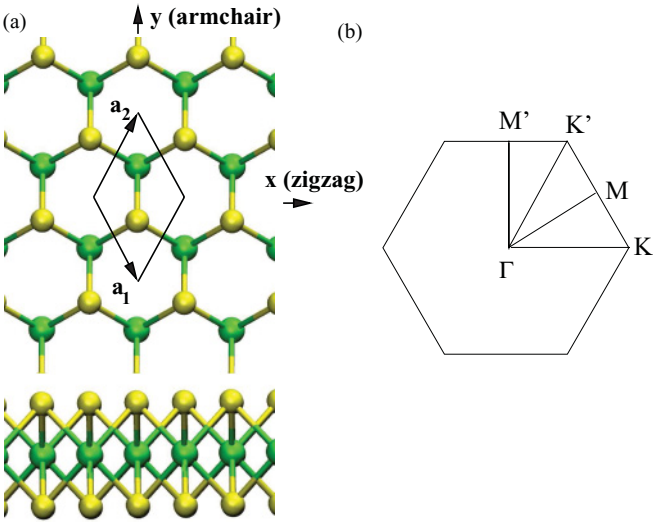

FIG. 1. (Color online) (a) The top view (top panel) and side view (bottom panel) of single-layer MoS_2. Mo and S atoms are represented by green and yellow balls, respectively. A unit cell with the in-plane basis vectors $\vec{a}_1$ and $\vec{a}_2$ contains three atoms. The x and y directions correspond to the zigzag and armchair directions, respectively. The corresponding first Brillouin Zone is shown in (b). Under uniaxial tension, the original crystal symmetry is broken, thus M' and K' become no longer equivalent to M and K.

isotropic 2D material. The elastic properties of single-layer[13] and multilayer MoS_2[13,14] have been recently measured by two nanomechanical experiments independently, both using atomic force microscope tip as an indentor applied on the MoS_2 mono- or multilayers suspended on the substrate with arrays of holes of micrometers in diameter. Under such experimental conditions, the MoS_2 layers are most likely under biaxial tensile stress. Bertolazzi *et al.*[13] obtained an effective Young's modulus of 270 ± 100 GPa for monolayer MoS_2, while Castellanos-Gomez *et al.*[14] obtained an average

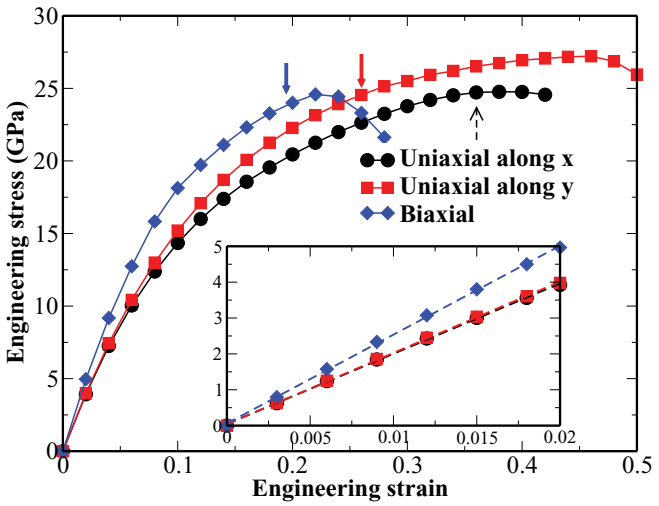

FIG. 2. (Color online) Calculated ideal tensile stress versus engineering strain for single-layer MoS_2. The solid and dash arrows indicate the onset strains for phonon instability and elastic instability, respectively. Insert shows the linear regression of the initial stress strain curves for obtaining the corresponding elastic moduli.

of 330 ± 70 GPa for MoS_2 nanosheets consisted of 5 to 25 layers. Our predicted biaxial elastic modulus E_{2D} (250.2 ± 5.8 GPa) is in an excellent agreement with the experimental data.

As the applied strain increases, the calculated stress-strain behaviors become nonlinear and show difference between the x and y directions. In particular, along y direction, both the maximum stress and its corresponding strain are higher than those along x direction. Based on the calculated stress strain curve alone, it appears that single-layer MoS_2 is stronger along y, namely, armchair direction. However, one needs to verify whether the single-layer MoS_2 remains stable before approaching the maximum stress, as orthogonal elastic instability[19,22,23] or dynamical instability[24,25] may intrude prior to the maximum stress on the strain path.

To examine stability conditions, we calculated the phonon dispersions for single-layer MoS_2, based on density functional perturbation theory.[26] The phonon dispersion for the stress-free state is shown in Fig. 3(a). In comparison with the recent calculation[27] based on local density approximation (LDA), our calculated phonon frequencies at Γ are slightly smaller, but the differences are within 4%. Two out of three acoustic branches correspond to vibration within the plane [longitudinal acoustic (LA) and transverse acoustic (TA)], and the other corresponds to vibration out of the plane (ZA). At the uniaxial tensile strain $\varepsilon_{yy} = 0.28$, a phonon branch has the negative (imaginary) frequencies near the M' point [Fig. 3(d)]. Similarly, at the biaxial tensile strain $\varepsilon_{2D} = 0.195$, a phonon branch becomes unstable near the K point [Fig. 3(b)]. Examination of the eigenvectors of the unstable phonon modes shows that both branches are ZA, corresponding to vibration out of the plane. In contrast, such phonon mode remains stable under uniaxial tension along x when reaching the maximum tensile stress. Figure 3(d) further indicates soft phonon near the Γ point at the critical tensile strain $\varepsilon_{xx} = 0.36$. Examination of the eigenvectors showed that the nature of this long-wavelength soft phonon mode is that the single layer becomes unstable with respect to a uniform tensile strain along x direction. In other words, the single-layer MoS_2 reaches its ideal tensile strength under uniaxial tension along x direction, due to the failure mechanism being the loss of elastic stability.

Table I summarizes the calculated ideal tensile strengths along all three loading directions. The predicted ideal strength is in an excellent agreement with the experimental average strength 22 ± 4 GPa.[13] Interestingly, single-layer MoS_2 appears virtually elastically isotropic if one only takes into account the predicted elastic moduli and the ideal strengths. However, the calculated critical strain and phonon instability indicate that the failure mechanisms upon tension in fact depends on the loading direction and the stress state.

TABLE I. Summary of the predicted elastic moduli, ideal strengths, critical strains, and failure mechanisms of single-layer MoS_2 under three strain paths.

Direction	E (GPa)	σ^c (GPa)	ε^c	Failure mechanism
x	197.9 ± 4.3	24.7	0.36	Elastic instability
y	200.3 ± 3.7	25.1	0.28	Phonon instability
Biaxial	250.2 ± 5.8	23.8	0.195	Phonon instability

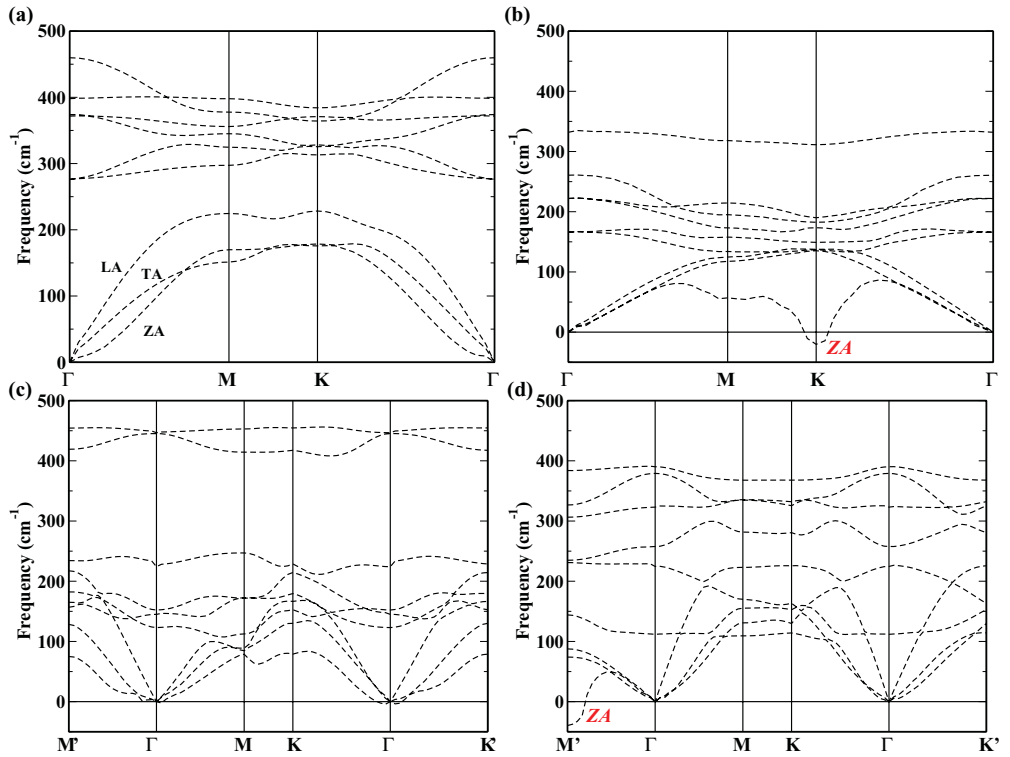

FIG. 3. Calculated phonon dispersion for single layer MoS_2 at (a) stress-free state, and at the critical strain under (b) biaxial tension with $\varepsilon_{2D} = 0.195$, (c) uniaxial tension along with x direction $\varepsilon_{xx} = 0.36$, and (d) uniaxial tension along with y direction $\varepsilon_{yy} = 0.28$. Under uniaxial tension, the phonon dispersion is plotted along $M' - \Gamma - M - K - \Gamma - K'$. Under both (b) and (d), the unstable phonon mode at the Brillouin Zone edge is identified to be the out-of-plane transverse phonon branch ZA.

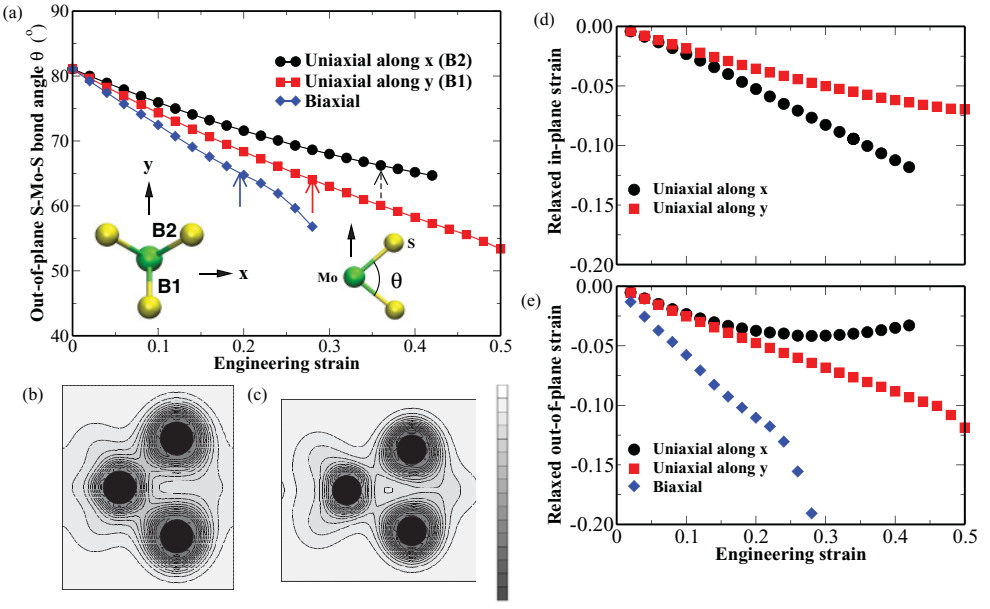

FIG. 4. (Color online) (a) The variation of the highest-load out-of-plane S-Mo-S bond angle θ with respect to the applied tensile strain. The solid and dash arrows indicate the onset of the out-of-plane phonon instability and elastic instability, respectively. The lower-left insert shows the top view of a MoS_6 unit that is composed of three S-Mo-S planes, with one plane parallel to y (B1) and two planes angled with respect to y (B2). The lower-right insert shows the side view of the S-Mo-S plane. The charge density contour are shown for (b) B1 or B2 plane at the stress-free state and (c) B1 plane at the critical strain $\varepsilon_{yy} = 0.28$ under the uniaxial tension along y. Darker color corresponds to higher charge density, with linear scaling between zero (white) and 1.21 electron/Å^3 (black). The in-plane (d) and out-of-plane (e) strain relaxation are shown as functions of the applied engineering strain.

It is interesting to compare the mechanical responses of single-layer MoS_2 under tension with those of graphene. For graphene, previous calculation[20] showed the uniaxial tensile strength of graphene is dictated by elastic stability. Further study showed that under a generic stress state of tension,[25] the strength of graphene can be also limited by soft-mode phonon instability. However, the soft-mode phonon identified in such case is in-plane. In single-layer MoS_2, it is the out-of-plane phonon mode that plays the key role in the failure mechanism upon tension along the armchair (y) direction.

The distinction between single-layer MoS_2 and graphene in their responses to uniaxial tensile strain can be attributed to the difference in their atomic structures. While graphene is a truly 2D atomic system, single-layer MoS_2 is composed of three atomic layers. Upon in-plane tension, the elastic deformation of graphene only involves the change of in-plane C-C bond length and C-C-C bond angle. In contrast, the two planes of S atoms in single-layer MoS_2 become closer due to Poisson contraction, thus changing the out-of-plane S-Mo-S bond angle. The relaxed in-plane and out-of-plane strains are calculated as functions of the applied tensile strain [Figs. 4(d) and 4(e)]. In the limit of small strain where single-layer MoS_2 is elastically isotropic within the plane, we calculate both the in-plane Poisson's ratio $\mu_{\parallel} = -\varepsilon'_{yy}/\varepsilon_{xx} = -\varepsilon'_{xx}/\varepsilon_{yy}$ of 0.21 and the out-of-plane Poisson's ratio $\mu_{\perp} = -\varepsilon'_{zz}/\varepsilon_{xx} = -\varepsilon'_{zz}/\varepsilon_{yy}$ of 0.27, where the prime symbol denotes the relaxed strain. At the stress-free state, each Mo atom is bonded with six S atoms (with three Mo-S bonds above the Mo plane and three bonds below), which forms three equivalent S-Mo-S planes normal to the 2D prism plane [see Fig. 4(a)]. The out-of-plane S-Mo-S bond angle at the stress-free state is 81.1°. When a uniaxial tensile strain is applied, the original crystal symmetry is broken and the two S-Mo-S planes (B2) are no longer equivalent to the third plane (B1). In particular, the S-Mo-S bond angles that undergo sever distortion are on the B1 plane for uniaxial tension parallel to the B1 (x direction) and on the B2 plane for uniaxial tension normal to the B1 (y direction). Figure 4(a) shows the variation of such S-Mo-S bond angle as a function of the applied tensile strain under different strain paths. It can be seen that the S-Mo-S bond angle decreases the most upon biaxial tension and the least upon uniaxial tension along x. Interestingly, for both the uniaxial tension along y and biaxial tension, the single-layer MoS_2 becomes dynamically unstable when the out-of-plane S-Mo-S angle reaches about 64°, suggesting a lower limit for which the single-layer MoS_2 remains dynamically stable along the out-of-plane direction. The calculated charge density [Fig. 4(c)] at the critical strain $\varepsilon_{yy} = 0.28$ indicates that the Mo-S bond on the plane parallel to loading direction is indeed significantly weakened.

It is also interesting to understand how the electronic structure of single-layer MoS_2, particularly its band gap, varies with tensile strain. To this end, we calculated the electronic band structures of strained single-layer MoS_2 under different strain paths and found its gap decreases with the applied strain. Under uniaxial tension, the variations of band structures are very similar between x and y directions. This is not surprising as MoS_2 is virtually isotropic at small strain, as indicated by the calculated stress strain relations (see Fig. 2). Under biaxial tension, the decrease of band gap with strain is more prominent. Both the direct band gap, i.e., from the valence band top at K to the conduction band minimum at K [see Fig. 5(a)], and the indirect band gap, i.e., from the valence band top at Γ to the conduction band minimum at K, vary with the applied tensile strain linearly when the strain is small. By fitting the calculated band gap with respect to the tensile strain (<1%) via linear regression, we obtained the linear strain coefficients of -44.4 ± 1.5 meV/% and -112.2 ± 4.2 meV/% for the direct band gap under uniaxial and biaxial tension, respectively, and the linear strain coefficients of -94.6 ± 2.2 meV/% and -239.4 ± 5.2 meV/% for the indirect band gap under uniaxial and biaxial tension, respectively. Figure 5 shows the calculated band structures under uniaxial tension along y and biaxial tension: The single layer MoS_2 already becomes an indirect semiconductor under biaxial tensile strain of 1%, whereas it remains a direct semiconductor at such strain under uniaxial tension. Band structure calculations also show that the lower bound of the band gap for which the single layer MoS_2 remains as a direct gap semiconductor is 1.68 eV, i.e., about 0.1 eV smaller than that of the unstrained single-layer MoS_2. At the larger strain, single-layer MoS_2 turns into metallic at a biaxial tensile strain of 9%, consistent with the recent finding,[28] while it remains an indirect gap semiconductor up to the critical strains under uniaxial tension along either direction.

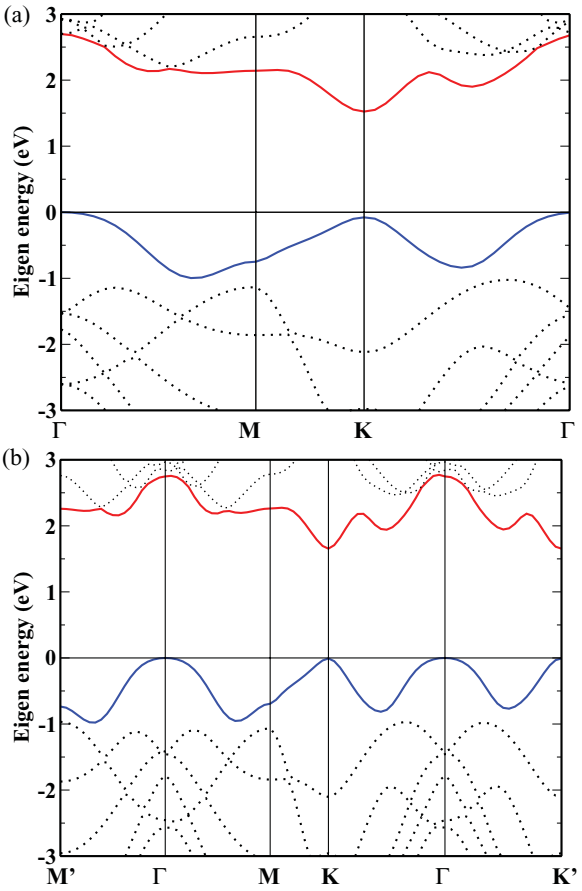

FIG. 5. (Color online) Calculated band structure of single-layer MoS_2 under (a) biaxial tension at $\varepsilon_{2D} = 0.01$ and (b) uniaxial tension along y direction at $\varepsilon_{yy} = 0.01$. The Fermi energy is set to be zero. The top valence band and bottom conduction band are highlighted by blue and red, respectively.

In summary, we investigated the elastic deformation behaviors of single-layer MoS_2 under both uniaxial and biaxial tension, by first-principle calculations. The predicted biaxial ideal tensile strength and elastic modulus are in excellent agreement with the very recent experiments.[13,14] It is further identified that the tensile strength of single layer MoS_2 are dictated by out-of-plane soft-mode phonon instability under biaxial tension and uniaxial tension along the armchair direction. This failure mechanism, different from that predicted for graphene, is attributed to the out-of-plane atomic relaxation upon tensile strain. Our calculation also shows single-layer MoS_2 becomes an indirect semiconductor at small tensile strain ($< 2\%$), and turns into metallic before reaching the ideal tensile strength.

The author gratefully thanks G. Galli and D.C. Chrzan for fruitful discussions. The author thanks the Department of Civil and Environmental Engineering at the George Washington University for computing support.

*tsli@gwu.edu

[1] A. Splendiani, L. Sun, Y. Zhang, T. Li, J. Kim, C.-Y. Chim, G. Galli, and F. Wang, Nano Lett. **10**, 1271 (2010).
[2] K. F. Mak, C. Lee, J. Hone, J. Shan, and T. F. Heinz, Phys. Rev. Lett. **105**, 136805 (2010).
[3] K. Novoselov, D. Jiang, F. Schedin, T. Booth, V. Khotkevich, S. Morozov, and A. Geim, Proc. Natl. Acad. Sci. USA **102**, 10451 (2005).
[4] P. Joensen, R. Frindt, and S. Morrison, Mater. Res. Bull. **21**, 457 (1986).
[5] J. N. Coleman, M. Lotya, A. O'Neill, S. D. Bergin, P. J. King, U. Khan, K. Young, A. Gaucher, S. De, R. J. Smith, I. V. Shvets, S. K. Arora, G. Stanton, H.-Y. Kim, K. Lee, G. T. Kim, G. S. Duesberg, T. Hallam, J. J. Boland, J. J. Wang, J. F. Donegan, J. C. Grunlan, G. Moriarty, A. Shmeliov, R. J. Nicholls, J. M. Perkins, E. M. Grieveson, K. Theuwissen, D. W. McComb, P. D. Nellist, and V. Nicolosi, Science **331**, 568 (2011).
[6] T. Li and G. Galli, J. Phys. Chem. C **111**, 16192 (2007).
[7] B. Radisavljevic, A. Radenovic, J. Brivio, V. Giacometti, and A. Kis, Nature Nanotechnol. **6**, 147 (2011).
[8] Y. Yoon, K. Ganapathi, and S. Salahuddin, Nano Lett. **11**, 3768 (2011).
[9] G. Eda, G. Fanchini, and M. Chhowalla, Nature Nanotechnol. **3**, 270 (2008).
[10] K. S. Kim, Y. Zhao, H. Jang, S. Y. Lee, J. M. Kim, K. S. Kim, J.-H. Ahn, P. Kim, J.-Y. Choi, and B. H. Hong, Nature (London) **457**, 706 (2009).
[11] Y. Li, Z. Zhou, S. Zhang, and Z. Chen, J. Am. Chem. Soc. **130**, 16739 (2008).
[12] C. Ataca, H. Sahin, E. Akturk, and S. Ciraci, J. Phys. Chem. C **115**, 3934 (2011).
[13] S. Bertolazzi, J. Brivio, and A. Kis, ACS Nano **5**, 9703 (2011).
[14] A. Castellanos-Gomez, M. Poot, G. A. Steele, H. S. J. V. D. Zant, N. Agraït, and G. Rubio-Bollinger, Adv. Mater. **24**, 772 (2012).
[15] P. Giannozzi, S. Baroni, N. Bonini, M. Calandra, R. Car, C. Cavazzoni, D. Ceresoli, G. L. Chiarotti, M. Cococcioni, I. Dabo, A. D. Corso, S. de Gironcoli, S. Fabris, G. Fratesi, R. Gebauer, U. Gerstmann, C. Gougoussis, A. Kokalj, M. Lazzeri, L. Martin-Samos, N. Marzari, F. Mauri, R. Mazzarello, S. Paolini, A. Pasquarello, L. Paulatto, C. Sbraccia, S. Scandolo, G. Sclauzero, A. P. Seitsonen, A. Smogunov, P. Umari, and R. M. Wentzcovitch, J. Phys.: Condens. Matter. **21**, 395502 (2009).
[16] J. P. Perdew, K. Burke, and M. Ernzerhof, Phys. Rev. Lett. **77**, 3865 (1996).
[17] N. Troullier and J. L. Martins, Phys. Rev. B **43**, 1993 (1991).
[18] T. Li, J. W. Morris, and D. C. Chrzan, Phys. Rev. B **70**, 054107 (2004).
[19] T. Li, J. W. Morris, and D. C. Chrzan, Phys. Rev. B **73**, 024105 (2006).
[20] F. Liu, P. Ming, and J. Li, Phys. Rev. B **76**, 064120 (2007).
[21] P. Young, J. Phys. D: Appl. Phys. **1**, 936 (1968).
[22] J. Morris and C. Krenn, Philos. Mag. A **80**, 2827 (2000).
[23] T. Li, J. W. Morris, N. Nagasako, S. Kuramoto, and D. C. Chrzan, Phys. Rev. Lett. **98**, 105503 (2007).
[24] D. M. Clatterbuck, C. R. Krenn, M. L. Cohen, and J. W. Morris, Phys. Rev. Lett. **91**, 135501 (2003).
[25] C. A. Marianetti and H. G. Yevick, Phys. Rev. Lett. **105**, 245502 (2010).
[26] S. Baroni, S. de Gironcoli, A. D. Corso, and P. Giannozzi, Rev. Mod. Phys. **73**, 515 (2001).
[27] A. Molina-Sanchez and L. Wirtz, Phys. Rev. B **84**, 155413 (2011).
[28] E. Scalise, M. Houssa, G. Pourtois, V. Afanas'ev, and A. Stesmans, Nano Res. **5**, 43 (2012).